Original Article

ZnO:CuO Nanocomposite Produced by Laser Ablation in Water for Antibacterial Activity

Zainab Ali Hrbe[1*], Muneer H. Jaduaa Alzubaidy[2], Ahmed N. Abd[3]

[1,2]Department of Physics, College of Science, Wasit University, Iraq. E-mail: zainabali@uowasit.edu.iq

[3]Department of Physics, College of Science, Mustansuria University, Iraq.

Abstract

Zinc oxide (ZnO) and copper oxide (CuO) nanoparticles were created using Nd-YAG pulse ablation, and they were subsequently examined as colloidal solutions. The produced nanoparticles were examined for UV-VIS absorption using transmission electron microscopy (TEM) and Fourier transform infrared spectroscopy (FTIR) (TEM). The production of zinc oxide and copper oxide nanoparticles is shown by FTIR characterization. the subsequent tests for UV-VIS absorption. According to TEM, the nanoparticle sizes varied from (30) nm for zinc oxide to (40) nm for copper oxide. X-ray diffraction was used to describe the films' structure (XRD)The X-ray showed the monoclinic crystalline structure of CuO and the hexagonal wurtzite phase of ZnO. Due to their antibacterial properties, copper oxide nanoparticles with a size range of 54.35–40.16 nm and zinc oxide nanoparticles with a size range of 36.16 nm were found to display FESM.

Keywords: Nanoparticles, laser ablation, XRD, SEM, antibacterial activity.

DOI: 10.47750/pnr.2022.13.S05.24

1. INTRODUCTION

In a rapidly developing area of materials science known as nanotechnology and nanoscience, particles with sizes between 1 and 100 nm and high surface-to-volume ratios are the focus [1]. Zinc oxide (ZnO) NPs have recently gained prominence due to their appealing and exceptional properties, such as high chemical stability, high photostability, high electrochemical coupling coefficient, and a broad range of radiation absorption, even though many NPs have shown their utility in various fields of technology [2]. ZnO NPs are n-type, multi-purpose semiconductors that operate at room temperature. They have a large band gap of 3.37 eV and high exciton binding energies of up to 60 meV [1]. The application of photocatalysts, biosensors, energy generators, and bio-imaging materials as well as antibacterial agents, vaccine delivery systems, and anti-cancer systems is increasingly widespread [3-5]. The production technologies used to create ZnO NPs include thermal hydrolysis operations, hydrothermal processing, the sol-gel method, the vapor condensation method, spray pyrolysis, and thermochemical approaches [6]. The process of creating nano-ZnO by irradiating a Zn target in liquid with high-energy laser pulses is known as pulsed laser ablation in liquid (PLAL) [7, 8]. As a result, the process is simple, economical, requires a small number of chemical species, and has a high level of control over the ablation atmosphere. Furthermore, because just the Zn target and water are employed for preparation, this technique is suitable for high-purity ZnO NPs [9]. One of these materials, copper oxide (CuO), is a P-type semiconductor with a band gap of 1.21–1.51 eV and is regarded as one of the favored oxides. With properties that cover every facet of materials in chemistry and physics, metal oxides are the most adaptable class of materials [10]. Additionally, the development of nanoscience and nanotechnology has created new opportunities to study the bactericidal effects of novel nanomaterials that contain metals known for their apparent bioactivity, such as Cu and Zn. Copper oxide semiconductors are known for their high optical absorption and non-toxicity [11-15]. The biological effectiveness of the material has been demonstrated to be significantly longer or higher than the (standard) bio-activity of the actual bulk metal in the majority of studies on metal-based nano-antimicrobials, which was believed to be the result of a variety of factors, including the non-traditional properties that are connected to the existence of the surface stabilizers, the size-dependent features of nano-metals, in addition to the high surface-to-volume ratio of ultrafine particles. It has been repeatedly demonstrated that capping chemicals modify the nanoparticle's ionic release and, consequently, its anti-biofilm properties. The requirement for clean living circumstances has led to new challenges in developing effective and economical antimicrobial materials that must be utterly harmless to humans and environmentally benign is currently promoting the effect of "smart" nano-antimicrobial [16]. In this research, two types of metal oxides were prepared by the method of laser ablation in water at one wavelength and compared them in terms of their biological properties and applications.

2. EXPERIMENTAL WORKS

Two types of metal powders (zinc and copper) of very high purity were used, and after grinding was carried out using a ceramic grinder and sifted them into very small particles, those powders were pressed with a manual press at a pressure of 5 tons for a period of 15 minutes to obtain solid tablets. The

water used in the experiment is distilled water (DW) with the chemical formula H2O, and the density is 1 g/cm3, and that one of its advantages is that it is a suitable solvent for most organic dyes and also a neutral solvent. Where were prepared glass bases with dimensions (2.5 x 2.5 x0.2) cm and were cleaned with distilled water and then dried with a special blotting paper, and then cleaned with high purity ethyl alcohol (99,99) for (15) minutes, then washed with a special blotting paper and then cleaned with distilled water after it cleans the floors to be ready, as shown in fig. 1, then the colloidal solution prepared by the (PLAL) method is deposited by distilling the colloidal solution onto those glass bases by using an electric heater at a temperature of (60) Celsius, so the liquid evaporates after NPS is deposited on the glass bases as shown in figure 2. The schematic diagram of laser ablation in a liquid system is shown in Fig. 1. Structural, morphological, and optical properties of ZnO, CuO and NPs, were investigated employing (CuKα) XRD-6000, Shimadzu X-ray diffractometer, Fourier transformation infrared spectroscopy, JEOL (JSM-5600) scanning electron microscopy, Philips CM10 PW 6020 transmission electron microscopy, Angstrom AA 3000 atomic force microscopy and Cary 100 Conc plus UV-Vis spectrophotometer. The colloidal ZnO and CuO nanoparticles were deposited on a glass substrate by drop casting.

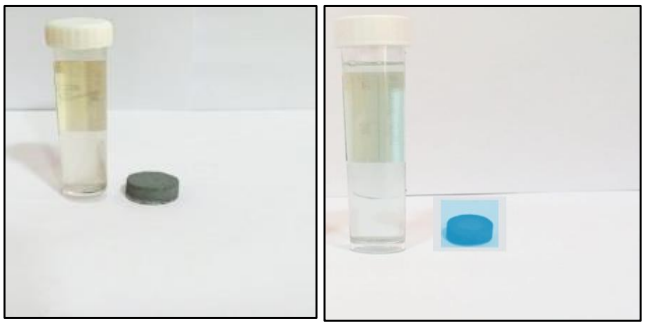

Figure 1: (a) Fresh colloidal ZnO NPs induce by Laser ablation in liquid and the ballet. (b) fresh colloidal CuO NPs induce by Laser ablation in liquid and the ballet (left to right).

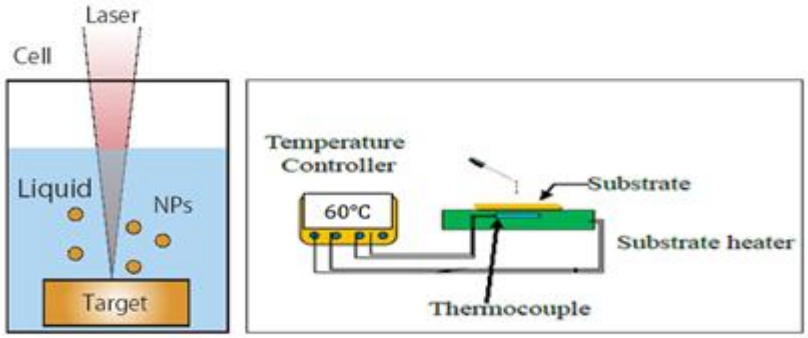

Figure 2: Shows laser ablation in liquid technique and precipitation of the solution on a glass substrate.

3. RESULTS AND DISCUSSION

Figure 2 displays the XRD spectra of the ZnO layer created by laser ablation and placed on glass using the drop-casting process at temperatures of 60 C.

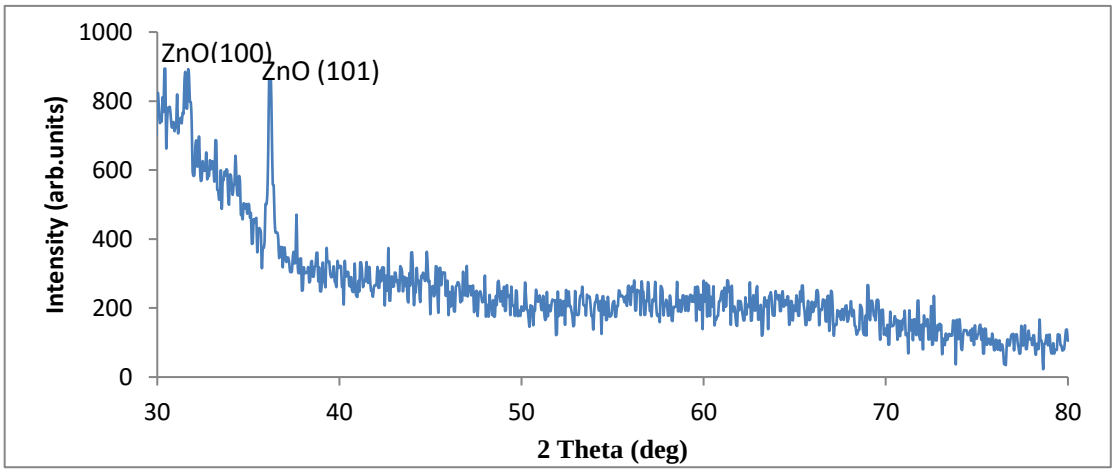

Figure 3: XRD pattern of synthesized ZnO nanostructure .

As part of our research program, we create nanoparticles with improved particle characteristics by employing chemical processes that aid surface energy control. The following procedures were used to identify the functionalized particles. X-ray Diffraction (XRD). The X-ray diffraction pattern of ZnO is shown in Figure 2. The produced material contains

particles with a size range in the nanoscale, according to a clear line widening of the XRD peaks. We were able to calculate the peak intensity, position, and width from this examination of the XRD patterns using full-width at half-maximum (FWHM) data. The hexagonal wurtzite phase of ZnO with lattice constants a = b = 0.324 nm and c = 0.521 nm has been accurately catalogued as the diffraction peaks at 31.84, 36.33, [17, 18]. (JPCDS card number: 1314-13-2) [19]. as indicated in Table 1, it also concurs with the researcher's findings (H.M. Jung). Since it only has ZnO peaks in its XRD profile, it is proof that the produced nanoparticle was free of contaminants. Using the Debye-Scherrer formula, the diameter of the produced ZnO nanoparticles was determined [20][21].

$$D_{av} = k\lambda/(\beta \cos\theta_B) \ldots.(1)$$

Where 0.89 denotes Scherrer's constant, λ is X-ray wavelength, and β full width at half maximum (FWHM) of the diffraction peak corresponding to plane 101,100 and θ Bragg diffraction angle. Using Scherrer's formula, it was determined that the sample's average particle size was 7.2 nm. This value is taken from the FWHM of the peak's more intense portion, which corresponds to the (101) planes and is positioned at 36.19.

. The dislocation density (δ) and the micro-strain (η), both measured in radial angles, were derived from the following two equations:

$$\delta = \frac{1}{D^2_{av}} \ldots.(2)$$

$$\varepsilon = \frac{\beta \cot\theta}{4} \ldots.(3)$$

Table :1 the structural characteristics calculated from the analysis of (ZnO) films using X-ray diffraction.

2θ (deg)	FWHM (degree)	d-spacing (Å)	D_{av}(nm)	δ $(nm)^{-2}$	ε	N◦ $(nm)^{-2}$
36.1916	0.2400	2.47998	7,2	0.02	$\times 10^{-5}$ 5.305	0.0968

As for copper oxide, Analysis of X-ray Diffraction at 60 °C Six major peaks can be found in the CuO,Cu2O,Cu XRD patterns at the following diffraction angles: 31.79, 36.36, 36.24, 43.44, 50.59 and 57.74 .respectively, for Copper oxides Observations are made and a comparison with the Joint Committee on Powder Diffraction Standards is made, . The film was made of polycrystalline materials. The standards peaks and the monoclinic structure were compatible (ASTM - Card file No. 34-1354,05-0661,02-1225,04-0836) [22].

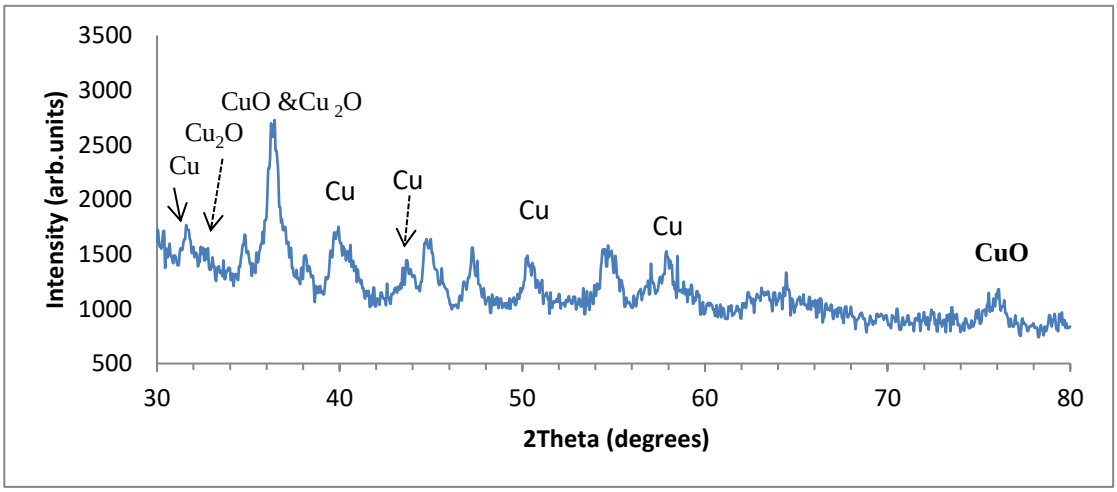

Figure4: X-ray diffraction of CuO nanoparticle

XRD analysis of the resultant solution and use of the Scherer equation to determine granular size. The average grain size for the thin films was 2.94 nm, which includes the XRD line width, which was estimated using the Sherrer equation [20].

The scanning electron microscope is considered the most important device used to study the surface of films with nanostructures to determine the size and shape of the particles that make up those surfaces. The preparation and deposition on the glass substrates were suitable for preparing and studying the films.. The other picture also indicates that those particles that make up the overlapping particles were of a semi-spherical shape with a diameter of no more than 36 nanometer, see figure 5:a. We note in Figure 5:b a very large difference in the size and shape of zinc oxide nanoparticles prepared by the laser ablation method in water with the same energy used to prepare the copper oxide particles, where we note that all the particles are spherical in shape and more homogeneous And the size of these particles does not exceed 34 nanometers.

Table 2: displays the structural characteristics calculated from the analysis of (CuO) films using X-ray diffraction.

	2θ (degree)	**FWHM (degree)**	**d-spacing (Å)**	**D_{av} (nm)**	**δ $(nm)^{-2}$**	**ε**	**N◦ $(nm)^{-2}$**	**Card No.**
Cu_2O	36.24	0.4920	2.47086	3.4	0.086	1.678×10^{-5}	1.0217	34-1354
CuO	36.3610	0.4920	2.47086	3.5	0.08	10.876×10^{-5}	1.102	05-0661
Cu	31.79	0.5904	2.82826	1.2	0.69	2.381×10^{-5}	23.24	02-1225
Cu	43.44	0.5904	2.07217	3.59	0.077	1.558×10^{-5}	0.8679	04-0836
Cu	50.59	0.4920	1.81386	2.97	0.1133	1.010×10^{-5}	1.532	04-0836
cu	57.74	0.3936	1.59003	3.03	0.1	0.62×10^{-5}	1.443	05-0661

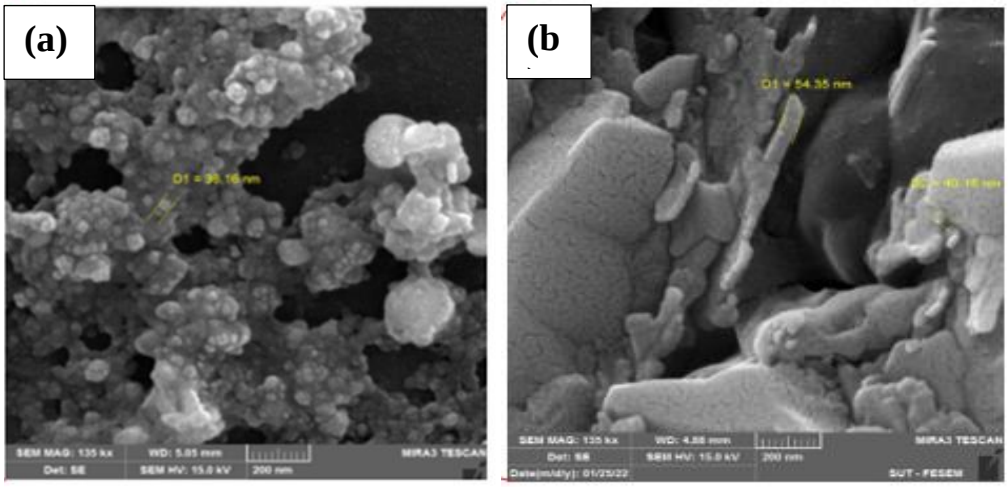

Figure 5: FE-SEM image of (a)copper oxide nanoparticles and (b) zinc oxide nanoparticles

Figure 6:a depicts a significant absorption peak discovered using FTIR analysis of copper oxide nanoparticles. This peak has four unique peaks, each of which has a different intensity. In the 1103.28/cm region that includes the C-O bond. And in the 663.51/cm region, that provides for the=C-H band, also in the1631.77/cm region, that provides for the c=c band. While OH stretched and encompassed the peak at 3317.56/cm, we observed a broadening at about (3317.56/cm due to OH's prolonged and vibrating mode. Due to its moisture absorption and the metallic oxide already present in the sample (682/cm), the curvature suggests the presence of water in the model. While FTIR Analysis FTIR spectroscopy is a very useful tool for investigating the vibrational properties of synthesized materials. The band positions and absorption peak not only depend on the chemical composition and structure of the thin films but the morphology of thin films also. FTIR spectrum of ZnO thin film is shown in Figure 6:b The absorption band observed at 532 cm−1 is attributed to the ZnO stretching vibrations [23]. Weak peaks at and 1612 cm−1 are attributed to symmetric and asymmetric C=O bond beats, respectively, and O-H at 3228 cm-1. The absorption peaks appearing at 2287 cm−1 are due to the absorption of atmospheric CO2 by metallic action [24].

The results of the TEM investigation revealed the creation of an "power-like cluster" of CuO nanostructure. The nanoparticles are stacked on top of one another, which greatly encourages the innovation of upper as well as a nanostructure. solution created by laser ablation is depicted in Figure 8 as a transmission electron microscope (TEM) picture. We observe from the TEM image that the development of NPs (ZnO) with a diameter of 10 to 80 nm reveals the quantitative size of ZnO nanoparticles, representing the form of rod particles. The size of the nanoparticles produced by the laser ablation process varies and depends on the solvent and the laser energy delivered.

Figure 8,a shows that CuO three-dimensional AFM pictures. The grains appear to be evenly spaced out and have distinct column grains that ascend to the top in the AFM picture. The total size of the pore grain was found to be roughly 243.6 nm using software and AFM analysis. The topography of the surface, including the mean roughness value and the root mean square, were also calculated. Figure8: b shows that AFM 3D surface topography CuO Nps films and average grain size range distribution. An atomic force microscope (AFM) was used to examine the surface's topography. The three-dimensional picture of ZnO nanoparticles showed a

population of uniform particles with a stable surface. In the liquid laser ablation process, ZnO nanoparticles have an average diameter of (357.9) nm. The surface's topography, such as the mean value of roughness and the root mean square.

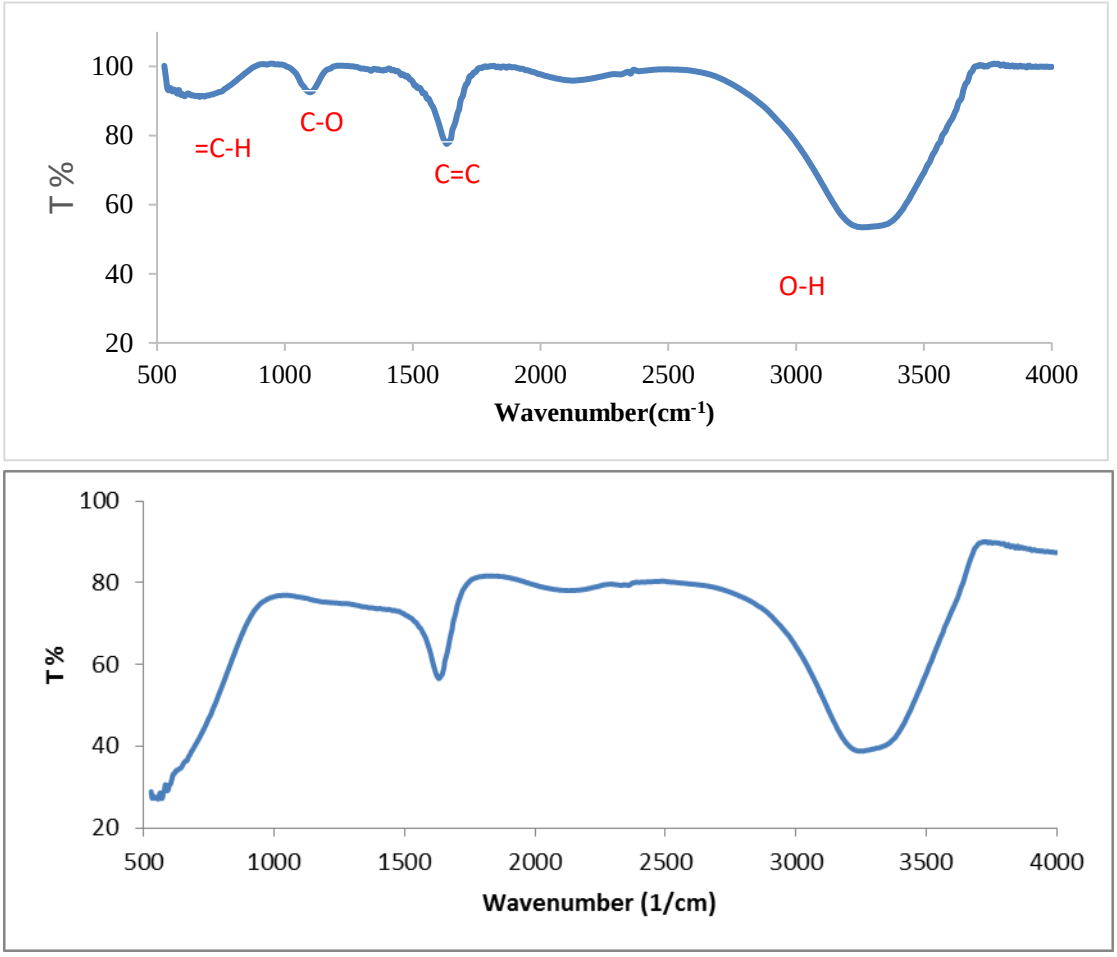

Figure 6: FTIR spectrum of (a) copper oxide particles and (b) zinc oxide nanoparticle.

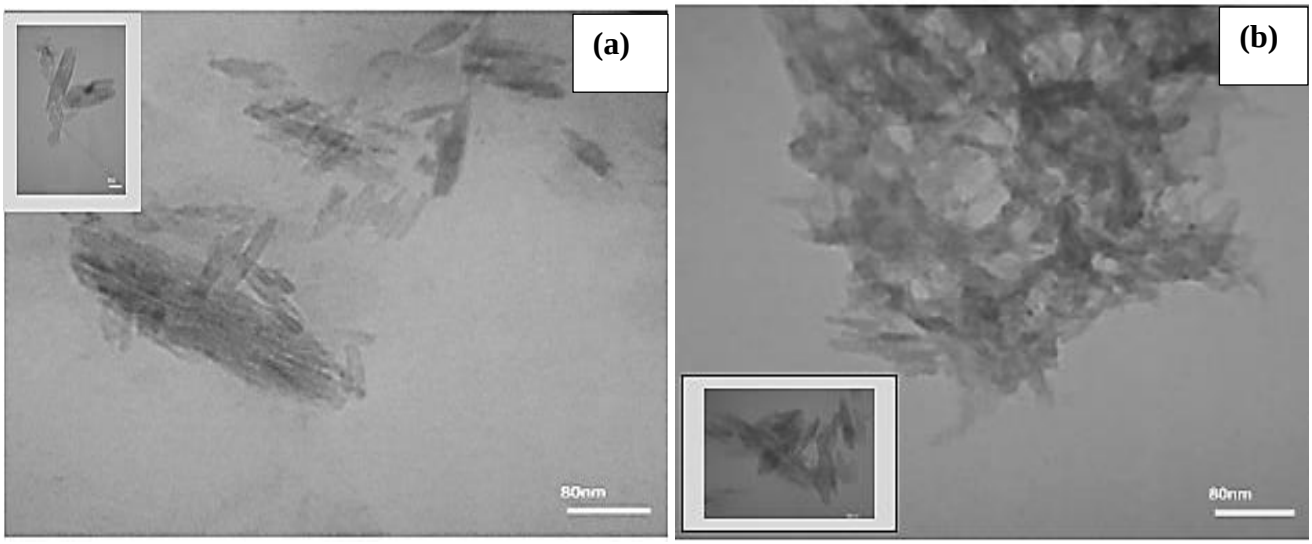

Figure 7: TEM image of nanoparticles of (a): copper oxide colloidal and (b). Zinc oxide colloidal.

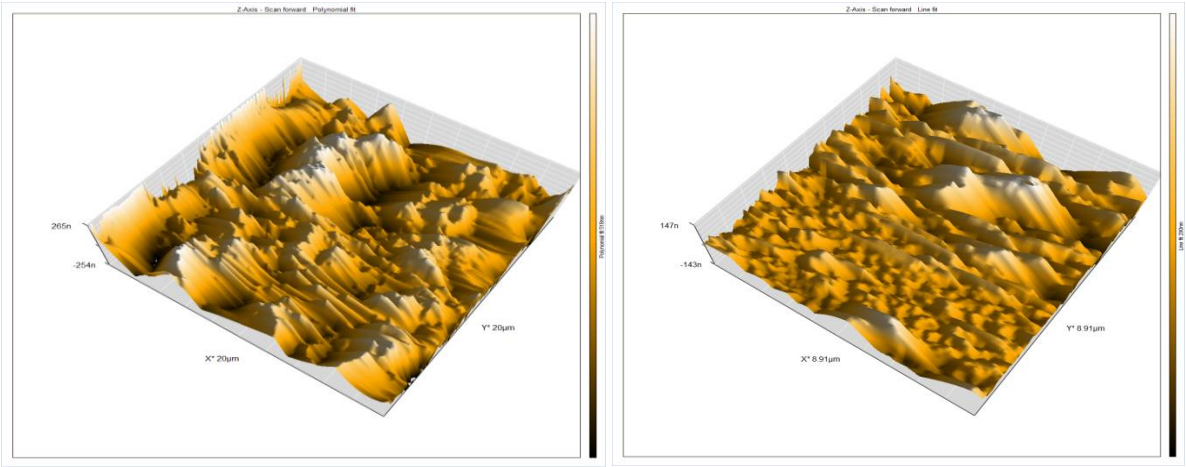

Figure 8: AFM 3D surface topography of CuO and ZnO Nps films.

Table (3) The average roughness, average diameter, and root mean square of the CuO and ZnO Nanoparticle films.

Sample	Average. Diameter (nm)	Surface Roughness (nm)	Root Mean Square (nm)
CuO	243.6	147-143	51.74
ZnO	357.9	265-254	183.1

According to the Copper's absorption spectrum, the absorption starts to decline at wavelengths around 200 nm. According to Figure 9, where its absorption is approximately (0.9%), it declines with increasing wavelengths in the visible (400-600 nm) and then increases where it is approximately (0.8%) in the infrared range [25]. Also,The absorption spectrum of zinc oxide nanoparticles (ZnO) prepared by the laser ablation method can be observed. It was shown that the absorption decreases at a wavelength of 200 nm. Where its absorption is about (0.8%) and then decreases with increasing wavelengths in the visible and infrared region [26] as see figures 9:a , b.

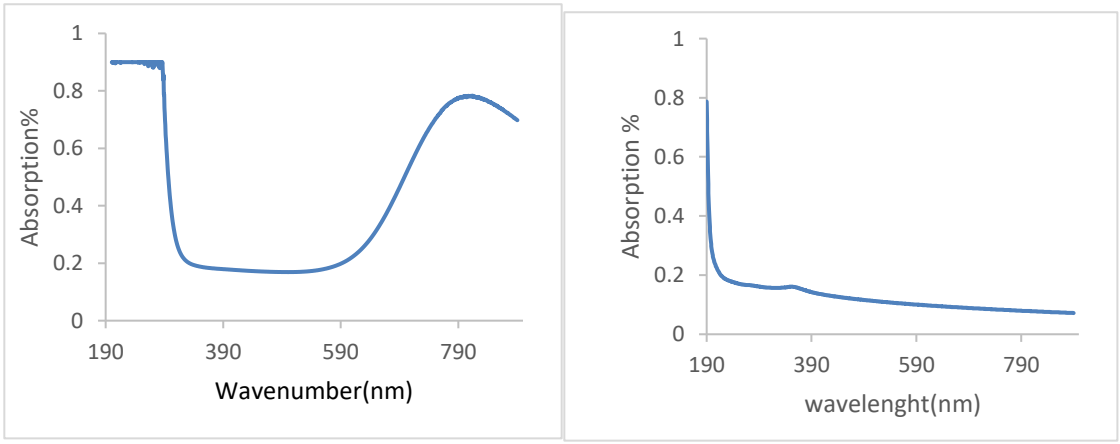

Figure 9: optical absorbance spectrum of (a) (CuO) nanoparticles and (b) (ZnO) nanoparticles

Figure 10. Shows the medium culture of bacteria E.coli, Pseudomonas aeruginosa, and S.aureus. The zone of inhibition is identified in the antibacterial test findings, as illustrated in Figure 4, indicating that ZnO-CuO nanocomposite particles are present.are efficient at destroying microbes ZnO-CuO nanocomposite compounds exhibit the greatest antibacterial activity, with an apparent zone for E.coli, 22 mm , S.aureus, 25 mm , S.epidermidis 25and for Klebsiella 22.[27] , listed in Table 4.

To quantify the quantity of absorbance and its interaction with this particular form of fungus, a nanocomposite - oxide substance created by laser ablation of liquid was added to the fungi. It can absorb up to 22mm.

The inhibition process may be brought on by particles penetrating the bacterial cell wall and occupying specific locations in the DNA helical structure, which stops metabolic processes and scatters enzymes, or it may be brought on by the attraction of nanomaterial ions at high concentrations to the bacterial cell wall, which limits oxidation and reduction and stops respiratory processes. To assess the quantity of absorbance and its interaction with this fungus, a nanocomposite copper oxide-zinc oxide substance made through laser ablation was introduced to the mixture of fungi. It can affect too.

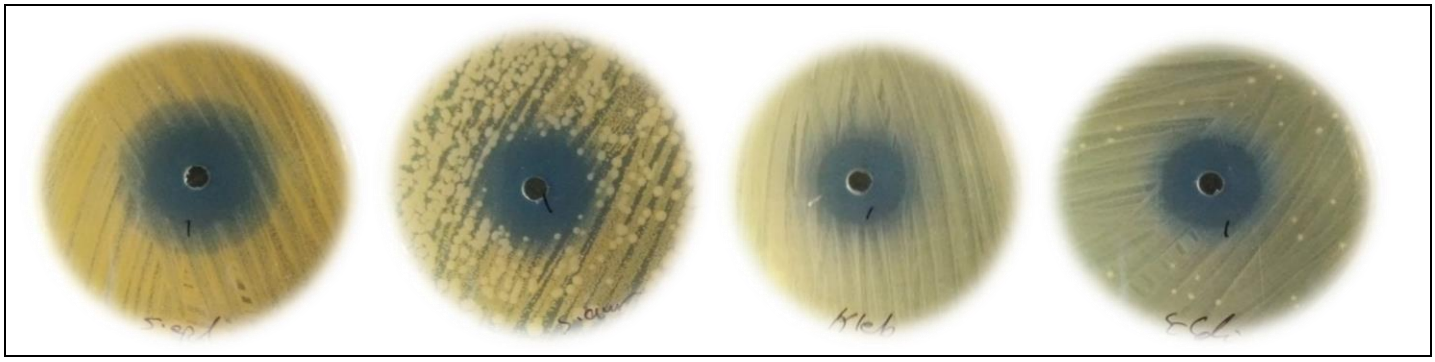

Figure 10: shows bacteria's adsorption of CuO:ZnO nanocomposite.

Table 4: Bacterial inhibition of CuO:ZnO nanocomposite.

Bacterial	Inhibition zone (mm)
S.aureus	25
S.epidermidis	25
E.coli	22
Klebsiella spp	22

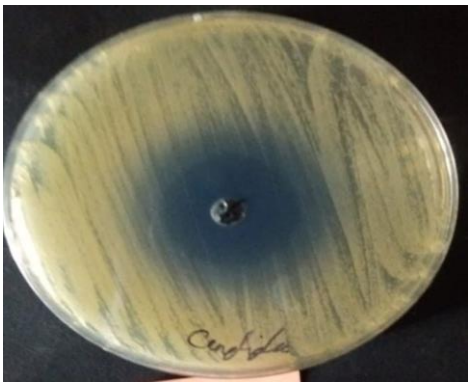

Figure 11: shows the amount of CuO:ZnO nanocomposite absorbed by fungi.

4. CONCLUSIONS

In this work, the laser ablation method was utilized to create copper and zinc oxide nanoparticles in water, which were then analyzed using XRD, SEM, TEM, UV-vis absorption, AFM, and FTIR. Laser ablation was used to create ZnO and CuO nanoparticles, which were then examined using XRD, SEM, TEM, UV-vis absorption, AFM, and FTIR. can produce nanoparticles of great abundance and good economic quality for the majority of metal oxides. Also the current study indicates that the rapid formation of zinc oxide and copper oxide nanoparticles by laser ablation of zinc and copper metal in water. may be detected in the UV-Vis absorption spectrum. FTIR spectra at a wavelength of (600-700) cm-1 demonstrate the relationship between zinc and oxygen, copper and oxygen. The results suggest that ZnO and CuO nanoparticles have an additive impact on bacterial cell membranes and that Zn and Cu nanoparticles may effectively boost bacterial penetration and absorption, making them a promising platform for biological applications. revealed that the effects of zinc oxide nanoparticles were not (Bacterial and fungi). Additionally, copper oxide nanoparticles had more of an impact on (Bacterial and fungi).

REFERENCES

Akimoto K, Ishizuka S, Yanagita M, Nawa Y, Paul GK, Sakurai (2008) T. Sol. Energy 0:715.

Alaa Z. Skheel , Muneer Hlail Jaduaa , Ahmed N. Abd "Green synthesis of cadmium oxide nanoparticles for biomedical applications (antibacterial, and anticancer activities) Materials Today: Proceedings 45 (2021) 5793–5799.

B. D. Cullity, Elements of X-Ray Diffraction, Addison-Wesley, Reading, Mass, USA, 3rd edition, 1967.

C.C. Trapalis, M. KokkOris, G. Perdikakis, G. Kordas, Study of antibacterial composite Cu/SiO2 thin coatings, J. Sol-Gel Sci Techn. 26 (2003) 1213–1218, https://doi.org/10.1023/A:1020720504942.

Chung Y T et al. 2015 Synthesis of minimal-size ZnO nanoparticles through the sol-gel method: Taguchi design optimization Mater. Des. 87 780–7

D.M Jahidul Haque , Md Masum Bellah, Md Rakibu Hassan and Suhanur Rahman" Synthesis of ZnO nanoparticles by two different methods & comparison of their structural, antibacterial, photocatalytic and optical properties" 1 (2020) 010007.

G. Faundez, M. Troncoso, P. Navarrete, G. Figueroa, Antimicrobial activity of copper surfaces against suspensions of salmonella enterica and campylobacter, BMC Microbial. 4 (2004) 19–25, https://doi.org/10.1186/ 1471-2180-4-19.

H.M. Jung, M.J. Chu, Synthesis of hexagonal ZnO nanodrums, nanosheets and na- nowires by the ionic effect during the growth of hexagonal ZnO crystals, J. Mater. Chem. 2 (2014) 6675–6682.

Ishikawa Y, Shimizu Y, Sasaki T, Koshizaki N (2006) Preparation of zinc oxide nanorods using pulsed laser ablation in water media at high temperature. J Colloid Interf Sci 300:612.

J. Zhou, F. Zhao, Y. Wang, Y. Zhang, and L. Yang, "Size- controlled synthesis of ZnO nanoparticles and their photolu- minescence properties," Journal of Luminescence, vol. 122-123, no. 1-2, pp. 195–197, 2007.

K.B. Holt, A.J. Bard, Interaction of silver(I) ions with the respiratory chain of Escherichia coli: an electrochemical and scanning electrochemical microscopy study of the antimicrobial mechanism of micromolar Ag+, Biochemistry 44 (13214–13223) (2005), https://doi.org/10.1021/bi0508542.

Kolodziejczak-Radzimska A and Jesionowski T 2014 Zinc oxide-from synthesis to application: a review Materials (Basel) 7 2833–81

M. Kawashita, S. Tsuneyama, F. Miyaji, T. Kokubo, H. Kozuka, K. Yamamoto, Antibacterial silver-containing silica glass prepared by sol-gel method, Biomaterials 21 (4) (2000) 393–398, https://doi.org/10.1016/S0142-9612(99) 00201-X.

R.K. Swarnkar, S.C. Singh, R. Gopal, Paper presented at the 1st International Conference on Nanostructured Materials and Nanocomposites, Kottayam, India, 6–8 April 2009.

Reddy K M et al 2007 Selective toxicity of zinc oxide nanoparticles to prokaryotic and eukaryotic systems Appl. Phys. Lett. 90 10–13.

Rekha K et al 2010 Structural, optical, photocatalytic and antibacterial activity of zinco xide and manganese doped zinc oxide nanoparticles Phys. B Condens Matter 405 3180–5

S. Pal, Y.K. Tak, J.M. Song, Does the antibacterial activity of silver nanoparticles depend on the shape of the nanoparticle? A study of the gram-negative bacterium Escherichia coli, Appl. Environ. Microb. 73 (6) (2007) 1712–1720, https://doi.org/10.1128/AEM.02218-06.

Sasaki T, Shimizu Y, Koshizaki N (2006) Preparation of metal oxide-based nanomaterials using nanosecond pulsed laser ablation in liquids. J Photochem Photobiol A: Chem 182:335

Siddiqi, K.S., A. ur Rahman and A. Husen (2018). Properties of zinc oxide nanoparticles and their activity against microbes. Nanoscale research letters., 13(1): 141.

Singh S, Gopal R (2008) Synthesis of colloidal zinc oxide nanopar- ticles by pulsed laser ablation in aqueous media. Physica E 40:724

Sirelkhatim, A., S. Mahmud, A. Seeni, N.H.M. Kaus, L.C. Ann,S.K.M. Bakhori, H. Hasan and D. Mohamad (2015). Review on zinc oxide nanoparticles: antibacterial activity and toxicity mechanism. Nano-Micro Letters., 7(3): 219-242.

Talebian N, Amininezhad S M and Doudi M 2013 Controllable synthesis of ZnO nanoparticles and their morphology-dependent antibacterial and optical properties J. Photochem Photobiol B Biol. 120 66–73

V. Sambhy, M.M. MacBride, B. Peterson, A. Sen, Silver bromide nanoparticle/ polymer composites: dual action tunable antimicrobial materials, J. Am. Chem. Soc. 128 (2006) 9798–9808, https://doi.org/10.1021/ja061442z.

Y. J. Kwon, K. H. Kim, C. S. Lim and K. B. Shim, "Charaterization of ZnO Nanopowders Synthesized by the Polymerized Complex Method via an Organochemical Route," Journal of Ceramic Processing Research, Vol. 3, June 2002, pp. 146-149 .

Yan X and Xu G 2009 Effect of sintering atmosphere on the electrical and optical properties of (ZnO)1-x(MnO2)x NTCR ceramicsPhys. B Condens Matter 404 2377–81

Yoon KH, Choi WJ and Kang DH (2000) "Photoelectro-chemical Properties of Copp.er Oxide Thin Films Coated on an n-Si Substrate," Thin Solid Films, 372(1- 2):250-256.

Z. M. Khoshhesab, M. Sarfaraz, and M. A. Asadabad, "Prep- aration of ZnO nanostructures by chemical precipitation method," Synthesis and Reactivity in Inorganic, Metal-Organic and Nano-Metal Chemistry, vol. 41, no. 7, pp. 814–819, 2011.